O. Alelweet, S. Pavia (2022) 1st
International Conference on
Environmental Science & Green Energy.
October 24-26 , 2022 Clichy, Paris.

Article

Suitability of a high-calcium slag for alkali activation, and strength and microstructure of the resultant materials.

Omar Alelweet [1], Sara Pavia [2,*]

[1] Department of Civil Engineering, University of Dublin Trinity College, IRELAND
[2] Department of Civil Engineering, University of Dublin Trinity College, IRELAND
* pavias@tcd.ie

Abstract: We study the feasibility of producing building materials by activating an Irish slag with alkali-metal activators. The slag is highly amorphous and basic (CaO+ MgO/SiO_2=1.56), with CaO/SiO_2=1.41 and Al_2O_3/SiO_2=0.34 which evidence high reactivity and potential for alkali activation-AA-. Its chemical composition complies with standard requirements for slags in concretes/mortars/grouts. Devitrification, supported by calorimetry, evidenced that the slag consists of a melilite-gehlenite isomorphous solution which denotes high reactivity. The slag was activated with NaOH and Na_2SiO_3, both combined and separately, to produce mortars. The mortars achieved reasonable setting times and workability, and strenght significantly increased between 28 and 270 days. Cracking by drying shrinkage, a challenge in AA materials, is hindered by the slag's high calcium. The Na_2SiO_3 + NaOH slag mortars gained the greatest compressive and flexural strengths. Rising the curing temperature to 60°C, enhanced their strength and microstructure (mainly up to 28 days), and develops hydrogarnet–gehlenite hydrate cements that may be responsible for the high 270-day strength (96MPa). Generally, curing at 60°C enhances early strength (3-7 day) but the increase between 28 and 270 days is not significant, with sometimes lower values than ambient-cured material (Na_2SiO_3-activator). An excessive %Na_2O by mass of slag is blamed for the low strength generated by the Na_2SiO_3 activator (the slag's high reactivity requires lower %Na_2O). The NaOH-activated slags tend to perform best when ambient-cured. An undue high molarity of the NaOH solution has generated an excessive alkalinity for the highly reactive slag, lowering the strength of the NaOH-activated slag mortars. The results indicate that the best activator is a combination of Na_2SiO_3 and a low molarity (<6M)NaOH.

Keywords: Ground Granulated Blastfurnace Slag - GGBS; alkali activation; devitrification; strength, hydrogarnet–gehlenite hydrate cement.

1. Introduction

Alkali-activated materials (AAMs) are usually produced with lower carbon emissions and less raw material and fossil fuel consumption than traditional Portland cement (PC) products. The reduction in emissions, and the use of waste for their production, may now become the trigger for their wide uptake in the markets. Ouellet-Plamondon and Habert [1] state that the environmental impact of current mixes is lower than cement/concrete made with 100% PC, saving up to 75% CO_2 emissions and having additional environmental benefits such as the reduction of water use, and no requirement for superplasticizer admixtures. The authors reviewed and standardised sustainability calculations based on life cycle analyses (LCA), highlighting the disparity of results, and

discussing the critical points that need to be addressed in order to improve the LCA of AA cements and concretes.

AA mortars and concretes consist of a silicate precursor which is activated with an alkali-metal and mixed with aggregate. It is important to use precursors that do not require calcination or any other high-energy processing for production. Also, it should be noted that certain activators such as sodium silicate can contribute up to 80% of the total impact of an AA material [1]. The precursors are either natural or man-made aluminosilicates, and they can be cementitious materials with hydraulic properties or pozzolanic. This research uses an Irish GGBS as a precursor. It is activated with sodium hydroxide (NaOH), and sodium silicate (Na_2SiO_3) which are considered as best activators according with the literature [2-4]. The alkali solution dissolves the slag generating Si^{4+}, Al^{3+} and Ca^{2+} cations that become available to form C-A-S-H cementing gels (main reaction product), a C-S-H cement with a high-level aluminium substitution [2-4].

Slags have been used for the production of AAs for decades. They were patented in 1958 and used in construction, in 1960 in USSR, and as precast products in Eastern Europe, Finland and France [5]. Some AA slag materials show advantages over PC products including: early hardening, high strengths, lower hydration heat, better resistance to water solubility, chemical attack (resistance to sulfates and chlorides) and carbonation, higher resistance of interfaces and a higher resistance to frost action [4]. However, they don't meet existing standards, and they can show too rapid setting, high shrinkage, and a tendency to expansive ASR (alkali-silica reaction), alkali-aggregate reactions (AAR) and salt efflorescence [2-5]. Further disadvantages can include unpleasant handling, skin irritation, inconvenience of mixing more than 2 components, sticky consistency [5]. Some of the challenges of AA cements and concretes are comprehensively summarised in Shi et al. [2] including: the appearance of alkali carbonate efflorescence due to the leaching of alkalis and their reaction with atmospheric CO_2; cracking due to drying shrinkage (which increases as the lime content in the system lowers); and the potential expansion by AAR. Shrinkage can prevent a wide range of applications for AA materials. However, for certain activators such as fly ash, it could be reduced significantly with heat curing [3].

The chemical and physical characteristics of the precursors (which vary from source to source) need to be determined and controlled to ensure the quality and consistency of AA materials. One of the restrains that inhibit the worldwide, production of AA cements is the uneven nature of the precursor required to manufacture them [2-4]. Furthermore, in AA cement design, the type of activator is essential because it impacts the properties and durability of the final product. Hence, it needs to be chosen based on the chemical composition and physical-chemical properties of the precursor [3-4]. This paper intends to contribute to this important quality control by investigating the composition and properties of an Irish slag, as a potential precursor, to produce AA cements. It determines how the slag can be best activated by investigating materials fabricated with different alkali activators. The paper studies the setting times, strength and structure of the resultant materials, with a focus on the effect of curing time and temperature.

The properties of the final AA material largely depend on the type of alkali activator. Fernández–Jiménez et al. [6] experimentally proved that, in slag materials, the nature of the alkaline activator is the most significant factor that determines strength, overriding the effects of the particle's specific surface area, curing temperature and activator concentration. When the alkali and the precursor are mixed, the pH controls reactivity because it determines the dissolution of the precursor. Previous authors state that silicate and hydroxides are the best activators for slags, because they generate the highest pH (or alkalinity) which accelerates the reaction between the activator and the precursor [2-4]. Hydroxide activators induce the hydrolysis of the Si-O-Si and Al-O-Al bonds releasing Si^{4+}

and Al^{3+}, and providing more hydroxyls than other activators, which raise the PH further than other activators, quickly reaching the values required for the dissolution of the precursor, and hence the formation of hydrate cements. Similarly, when activating a slag with silicate, the glassy phases disintegrate and the polycondensation reaction takes place whereby tobermolite and calcium silicate hydrate are generated at 1 day [7]. However, it has been noted that silicate activators provide a much higher level of available alkalinity over longer periods because, when a moderate amount of silica dissolves, the PH does not drop rapidly (as it is the case with hydroxide activators) [4].

A high pH is not considered suitable for Ca-rich precursors such as GGBS, because at very high OH^- concentrations, although silica and alumina increase solubility, calcium becomes less soluble [3]. Therefore, high-calcium slags (Ca=35-45%) are usually activated under moderated alkaline conditions [2, 6, 8]. Furthermore, high concentrations of hydroxide activator in GGBS have been reported to encourage efflorescence and increase cost [3-4]. It is considered in the literature that slags can be successfully activated with a combination of alkali hydroxide and silicate. The fluidity of the hydroxide activator maintains a suitable rheology while the silicate provides Si ions for the generation of cementing hydrates that contribute to strength [3]. The proportion of NaOH / Na_2SiO_3 is essential as NaOH acts as dissolvent while Na_2SiO_3 acts as a binder [9].

It is well known that the reactions of the non-clinker phases of AA materials are slower than the clinkers in PC materials, and that the binding of water is generally slower and/or weaker than in the Ca-rich, C-S-H phases of PCs. Therefore, it is even more important to control curing conditions in AA binders [4]. Curing temperature is considered an important parameter, and it is the most widely investigated. However, the optimal curing temperature depends on the slag properties and composition and the mix design, and it is generally agreed that an extended curing time is also important to develop a durable material. The curing temperature influences the strength development of AA slag mortars. Significant retardation at 5°C, and significant acceleration at 40°C compared with curing at 20°C have been reported [10]. Heat curing typically enhances early strength of AA slag materials, but the late strength is significantly reduced when compared with room temperature curing [11]. Bakharev et al. [11] note that curing at 60°C is the most effective method for Na_2SiO_3 -activated slags. They also note that when slags are activated with a combination of Na_2SiO_3 and NaOH, curing at 70°C accelerates early strength development but, after 28 days, the strength is 35-45% lower than the strength of the ambient-cured specimens. However, Altan and Erdoğan [12] observed that AA slags activated with a mixture of Na_2SiO_3 and NaOH, cured at room temperature for a sufficiently long time, will reach the same strength or greater than when cured at 80°C.

The chemistry and mineralogy of any pozzolanic or cementing material (mainly its amorphous content), as well as its fineness and the specific surface area of its particles, control the formation of reaction products (cements) which consequently define the properties of the end materials. Reactivity increases proportionally to the slag's fineness and specific surface area (SSA). The chemical composition of the slag and the activator affect the nature of the resultant cement, and hence the properties of the material. In high-calcium materials such as GGBS, the principal reaction product of alkali activation is a C-A-S-H gel (C-S-H with a high-level Al substitution), similar to the gel obtained on PC hydration [13, 14, 3, 15] which determines mechanical strength and durability. The CaO/SiO_2 reactive ratio controls the characteristics of the C-A-S-H gel [3]. Adding soluble silica to the system, e.g. using a sodium silicate activator, alters the CaO/SiO_2 ratio leading to a denser microstructure with more polymerised gels and excellent mechanical properties (> 80 MPa at 28 days, [13, 14]. According to Wang et al [16], for slags, the available soluble silica is the most important parameter for alkali activation as it affects

workability, setting and strength. They state that important variables in alkali activation are the molar ratio SiO_2/Na_2O and the silica concentration.

The chemical composition of the slag and the activator further determines the resultant cement as evidenced by former authors: AFm phases appear as secondary reaction products when using NaOH as activator, whereas the Si-containing AFm phase strätlingite [17, 18] and hydrogarnets such as katoite [19] appear when using silicate as activator. Zhang et al. [7], activated a GGBS of chemical composition nearly identical to the GGBS in this paper but lower SSA (701 m^2/kg) and less amorphous (consisting of akermanite, gehlenite, calcium silicate and merwinite), with Na_2SiO_3 (waterglass, modulus = 1). On hydration, the authors found mainly C-S-H, epidotes and zeolites as follows: C-S-H at 1 day; gismondine ($CaAl_2Si_2O_8$ x $4H_2O$) at 3 days; zoisite ($Ca_2Al_3Si_3O_{12}$ OH) 7 days and wairakite ($CaAl_2Si_4O_{12}$ x $2H_2O$), natrolite ($Na_2Al2Si_3O_{10}$ x $2H_2O$) and clinozoisite ($Ca_2Al_3Si_3O_{12}OH$) at 28 days.

2. Materials and Methods

2.1. Physical properties and composition of the slag.

A GGBS made in Ringsend, Ireland, with raw molten slag imported from Europe, and a particle density of 1.80 Mg/m3 was used. The particle size distribution was measured by laser diffraction with a Mastersizer 2000 which records the angular distribution and intensity of the light reflected by the particles in suspension, and uses the Mie theory of diffraction to predict the particle size. The specific surface area (SSA) was measured with a Quantachrome Nova 4200e and the BET (Brunauer–Emmett–Teller) method which records the SSA based on the physical adsorption of gas molecules by the slag particles. The chemical composition of the GGBS was determined with X-ray fluorescence (XRF) analyses as a percentage by oxides using a ThermoFisher Scientific and Edwards Analytical with a Quant'X EDX spectrometer and a UniQuant analysis package. The loss on ignition (LOI) was measured as weight loss on calcination. The mineralogical composition and amorphous character of the slag, was assessed by X-Ray Diffraction (XRD) with the powder method, using a Phillips PW1720 XRD with a PW1050/80 goniometer and a PW3313/20 Cu K-alpha anode tube at 40kV and 20mA. The XRD results evidenced that the slag is highly amorphous, therefore, thermal treatments were used to cause phase transformation (devitrification) and hence determine the amorphous phases comprising the slag. In addition, thermal analyses were carried out with differential scanning calorimetry (DSC) and thermal gravimetric analysis (TGA).

2.2 Mixing, moulding and curing.

The slag was activated with sodium hydroxide (NaOH) and a commercial solution of sodium silicate (Na_2SiO_3). The activators were investigated separately and together (Table 1). The solid NaOH was dissolved into an 8M alkali solution. The silicate solution was mixed with the NaOH solution to provide extra Si ions. As aforementioned, the CaO/SiO_2 reactive ratio determines the characteristics of the resultant cements (C-A-S-H gel) [3], and adding soluble silica alters the CaO/SiO_2 ratio leading to a denser microstructure with more polymerised gels and enhanced mechanical properties [13, 14]. Therefore, the Na_2SiO_3 + NaOH activator was prepared, at a mass ratio of 1.5, based on an enhanced compressive strength previously reported [20]. The ratio between liquid and solid (water + alkaline solution / GGBS) was determined with the initial flow test (table 1). The amount of water+alkali solution required for the mortars to provide a suitable workability for handling and placing (a workable mix with a flow diameter of c.170 mm) was measured using a flow table - EN 1015-3 [21].

Several authors have demonstrated that the rheology of AA slag pastes depends on the activator used and that increasing the available soluble silica affects workability and setting of AA slag materials [2-4]. This was evidenced during mixing, as it can be seen from the table, the silica activator was less workable, requiring 60% of the water+alkali solution to reach a flow diameter of 168 mm while the Na_2SiO_3 + NaOH activated mortars only required 47%. The GGBS and sand were dry mixed at a ratio of 1 to 3 for 6 min, and later in a mixer for a further 3 min. The activator solution was then added and mixed for a further 5 mins. All the activators were in liquid form. NaOH was the most viscous and Na_2SiO_3 the stickiest. The filled moulds were vibrated according to the standards, and the specimens sealed with a plastic sheet to prevent moisture loss during curing. The specimens were demoulded after 24 hours and cured in ambient conditions for 24 hours. After this, some of the specimens were cured in an oven, at 60°C for 24 h, and then in ambient conditions for the rest of the time. The curing temperature was raised to 60°C as a catalyzer to enhance the alkali reaction and polymerization. However, it was kept low and with a short dwelling time (24h) due to environmental concerns.

Table 1. Composition of the alkali activated GGBS mortars.

Activator	GGBS (g)	Sand (g)	Na_2SiO_3/NaOH	8M NaOH(g)	Na_2SiO_3(g)	Water+alkali solution/GGBS
Na_2SiO_3/NaOH	500	1500	1.5	94	141	0.47
NaOH	500	1500	-	117.5	0	0.47
Na_2SiO_3	500	1500	-	0	300	0.60

2.3 Properties of the AA mortars.

As aforementioned, the amount of alkali solution required for the GGBS to provide suitable workability for handling and placing was measured with a flow table according to EN 1015-3 [21]. The setting time was measured according to EN 196-3 [22]. The compressive strength was measured in accordance with EN1015-11, using a ZWICK 1474 machine of 100 kN loading capacity, at a loading rate of 10N/s. The results reported are the arithmetic mean of six tests. The microstructure of the materials was assessed with a scanning electron microscope (SEM) and a petrographic microscope. These qualitative analyses focussed on the cement and the interface. Thin sections sized approximately 2 cm^3 were prepared for SEM analysis. SEM micrographs were captured, between 5 and 10kV, using an SE2 detector with a Karl Zeiss Ultra FESEM microscope. The ambient cured materials were investigated with a Field Emission Scanning Electron Microscope (FE-SEM) Tescan TIGER MIRA4 FE-SEM equipped with motorised Backscatter Electron (BSE) detector, and samples coated with 12 nm of carbon. A petrographic microscope was used to study the matrix and the transition zone at the interface. Thin sections were cut from representative hand samples, they were polished to the standard thickness of 20µm, and examined with both transmitted and polarised light, with low, medium and high-power objectives of 2×, 10×, 20x and 40× magnifications.

3. Results and discussion

3.1. Properties of the GGBS and suitability for alkali activation

In slags, fineness is a key factor influencing setting, strength development and the final microstructure of AAMs. Slag fineness and CaO content affect the fresh and hardened properties of the resultant AA materials [3]. Over a certain threshold, fineness can have an adverse effect on strength due to a higher water demand. The results (Table 2) evidenced that the slag is ultrafine, considerably finer than other AA slags [5]. Increasing

fineness leads to higher compressive strengths, especially at early ages, in AA slags [10; Križan et al. 2005 in [3]). However, it can shorten setting time [14,15]. Wang and Scrivener [23] and Puertas [24] suggest that the optimal fineness lies between 400 and 550 m^2/kg.

Table 2. Specific surface area and particle size of the GGBS.

	Specific surface area (SSA) m^2/kg	**Particle size**			
		Mean μm	D90 μm	D50 μm	D10 μm
GGBS	1950	Range: 0.25 to 75 μm 18.00	31.62	11.67	2.35
CEM II	1880	-			

The results of the chemical composition analyses (Table 3) evidenced that the GGBS is basic ($CaO+ MgO / SiO_2 >1 = 1.56$), therefore, it should have significant hydraulic activity on alkali activation. The more basic the slag the greater its hydraulic activity in the presence of alkali activators [25]. Glassy slags with CaO/SiO_2 ratios between 0.50 and 2.0, and Al_2O_3/SiO_2 ratios between 0.1 and 0.6 are considered suitable for alkali-activation [4]. The ratios in the slag investigated are 1.41 and 0.34 respectively, therefore it is suitable for alkali activation. Furthermore, the slag complies with the standard chemical requirements for the use of slags in concretes mortars and grouts (Table 4).

Table 3. Chemical composition as a percentage by weight. [a] same GGBS analysed by [26].

	SiO_2	Al_2O_3	CaO	Fe_2O_3	Na_2O	K_2O	MgO	P_2O_5	SO_3	Cl	TiO_2	MnO	LOI %	
													450 °C	1000°C
GGBS	31.71	10.83	44.90	0.51	0.03	0.71	7.50	0.42	2.08	0.03	0.95	0.17		
GGBS[a]	34.14	13.85	39.27	0.41	0.00	0.26	8.63	-	2.43	-	0.54	0.25	0.41	-0.77
Mean	32.00	12.00	42.00	0.45	0.03	0.5	8.00	0.42	2.2	0.03	0.75	0.20		

Table 4. Compliance of the GGBS with chemical standard requirements.

	SO_3-S^{2-} (%)	**MgO (%)**	**Cl^-**	**LOI (%)**	**Fineness m^2/kg**
EN 15167-1: GGBS requirements for use in concretes, mortars and grouts	≤ 2-2.5	≤ 18	≤ 0.10	≤ 3	≥275
GGBS	2.2	8	0.03	0.41	1950

The chemical composition of the slag influences the composition of the resultant cement. The high aluminium content of this slag can increase the level of substitution of Al in the C-A-S-H cement, principal product generated on AA. Considering the moderate Mg content of the slag, hydrotalcite can be expected (typically present in slags with high MgO content [13]) but no zeolites gismondine and garronite (typical of slag binders with high Al_2O_3 and low <5% Mg [27]). The chemical composition of the activator also affects the nature of the cement. Hence, AFm phases can be expected as secondary reaction products when using NaOH as activator, and the Si-containing AFm phase strätlingite and hydrogarnets such as katoite when using silicate as activator [17, 18, 19].

The mineralogy of the precursor, mainly its amorphous or vitreous phase content, determines reactivity, and hence the formation of cements which define the mechanical strength and durability of the resultant materials. The X-Ray diffraction trace (figure 1) shows that the GGBS is totally amorphous, including no crystalline phases. Therefore, the

silica and alumina in the slag are highly reactive, and can readily dissolve providing ions for cement formation.

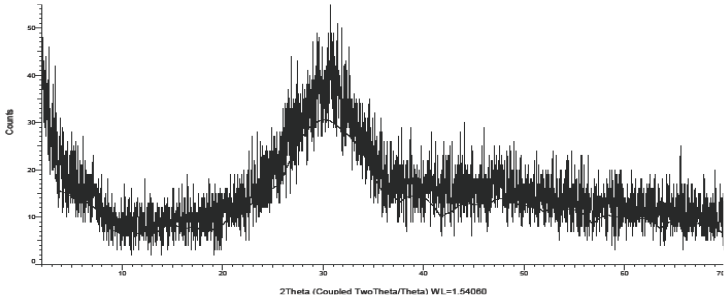

Figure 1. XRD trace of the slag with no crystalline phases and a marked halo which indicate total amorphousness.

Devitrification by thermal treatment caused phase transformation. The high amorphousness of the unheated slag was evidenced by the extended halo and the absence of crystalline phases in the XRD trace (figure 1). According to the devitrification results, at 500°C, the GGBS is still mostly amorphous, but a small amount of crystalline merwinite - $Ca_3Mg(SiO_4)_2$ - has begun to form (figure 2). Therefore, the transformation of the glass into crystals begins at approximately 500°C. At 800°C (figure 3), a significant crystalline fraction exists including merwinite and gehlenite -$Ca_2Al[AlSiO_7]$-: the amount of merwinite has increased and gehlenite has begun to form. Merwinite appears at 500°C, and is abundant at 800°C. However, at higher temperature, it is no longer stable and progressively transforms into gehlenite, so that at 1000°C, it has completely disappeared (figure 4), and the slag consists entirely of gehlenite. This mineral composition agrees with the literature [25].

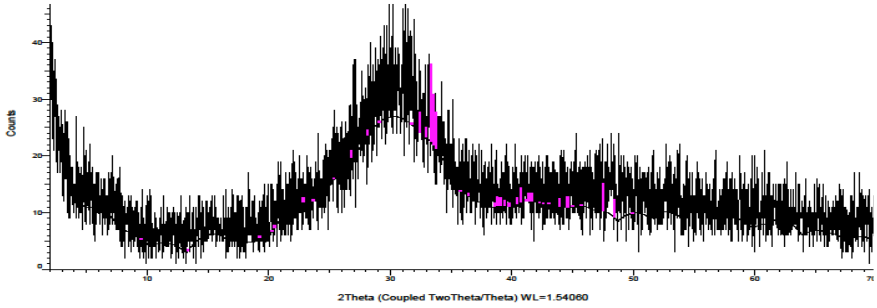

Figure 2. XRD trace of the slag at 500°C, the halo indicates that the slag is still highly vitreous but a small amount of crystalline merwinite $Ca_3Mg(SiO_4)_2$ has formed.

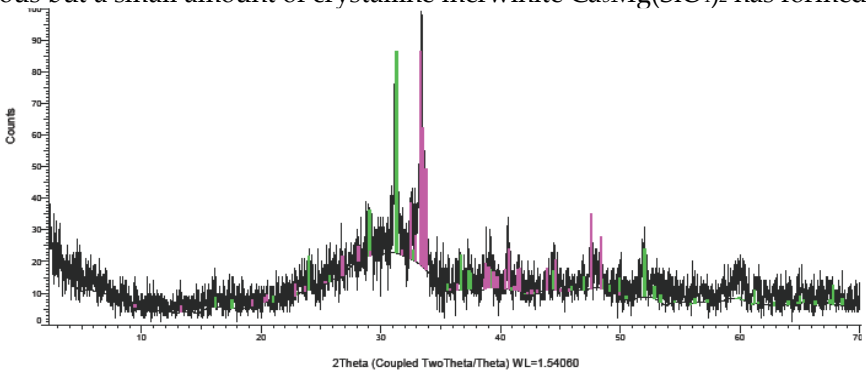

Figure 3. XRD trace of the slag at 800°C, the amount of merwinite has increased and gehlenite $Ca_2Al[AlSiO_7]$ begins to form.

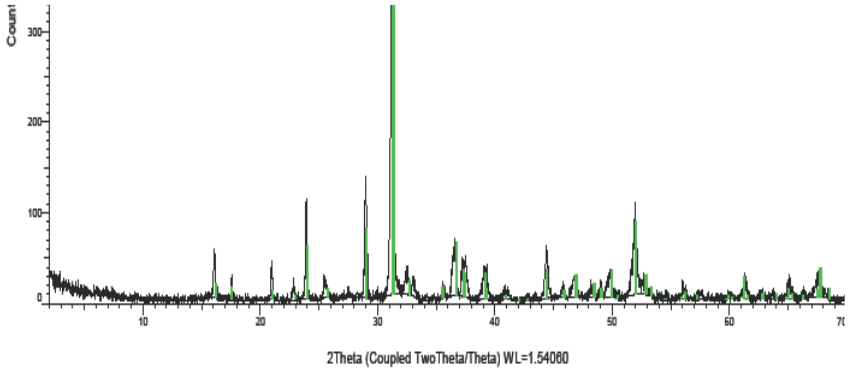

Figure 4. At 1000°C, the GGBS is completely devitrified, only gehlenite is stable, and merwinite has transformed into crystalline gehlenite.

The glass content of the GGBS at increasing temperature was calculated based on the background area determined by the lifting of the difractogram's baseline between 15 and 35 (2θ) which indicates the presence of amorphous materials (Table 5). The relative amounts of the crystalline phases were calculated using the relative intensities of their main reflexions: merwinite: 2Θ=33.38 with d-spacing= 2.68; and gehlenite: 2Θ=31.20 with d-spacing= 2.85 Å.

Table 5. Mineral composition and amorphousness of the GGBS. (*) calculated using the intensities of main reflexions: merwinite: 2Θ=33.38 / d-spacing= 2.68; gehlenite: 2Θ=31.20 / d-spacing= 2.85 Å.

Material	% Glass	% Crystalline	Mineral composition
GGBS 0°C	>90	<7	Glass. No crystals recorded.
GGBS 500°C	80-85	>7	Glass + traces of crystalline merwinite.
GGBS 800°C	c.11	50*	Merwinite $Ca_3 Mg (Si O_4)_2$
		38*	Gehlenite $Na_{0.05} Ca_{1.96} Mg_{0.24} Fe_{0.12} Al_{1.25} Si_{1.39} O_7$
GGBS 1000°C	<7	>90	Gehlenite $Na_{0.05} Ca_{1.96} Mg_{0.24} Fe_{0.12} Al_{1.25} Si_{1.39} O_7$

The thermal analyses by DSC and TGA mirror the results of the devitrification experiment. According to the DSC results (figure 5), a progressive exothermic DSC curve is observed between 0 and 500°C (the slag releases heat up to approximately 500°C). The devitrification results evidenced that, during this heat evolution, a small amount of crystals of merwinite appear but no major changes occur in the slag, which remains mostly amorphous (figure 1-2 and table 5). Above 500°C, the DSC curve becomes endothermic, and the GGBS keeps absorbing heat until it reaches 800°C. The devitrification test proves that the steady heat absorbed between 500 and 800°C is due to the decomposition of most of the glass to form crystalline merwinite and gehlenite (figure 3 and table 5). As indicated by the phase evolution during devitrification, the marked exothermic peak at 850°C likely corresponds to the transformation of merwinite into gehlenite, while the steady endothermic branch that follows (up to 1000°C) corresponds to the decomposition of the remining glass into crystalline gehlenite (figure 4 and table 5). The main events agree with previous authors who identified main endothermic peaks at 800°C and 1000°C, and attribute them to the devitrification of the GGBS [4]. However, when compared with other GGBS [28], the crystallization reactions are more progressive and steadier, taking place over a longer temperature range rather than suddenly, at specific temperatures. The mass of the GGBS remains nearly constant up to 1000°C, with a slight mass loss (1%) and a final slight mass increase. This indicates that the GGBS does not include either constitutional water or organic carbon or carbonates, supporting the LOI results (Table 3), and the chemical and mineralogical analyses (Tables 3 and 5). After reaching 850°C, the GGBS gains a slight

mass. The devitrification experiment indicates that this is probably due to the conversion of merwinite Ca3Mg (SiO4)2 into denser gehlenite Ca2Al [AlSiO7] (Table 5).

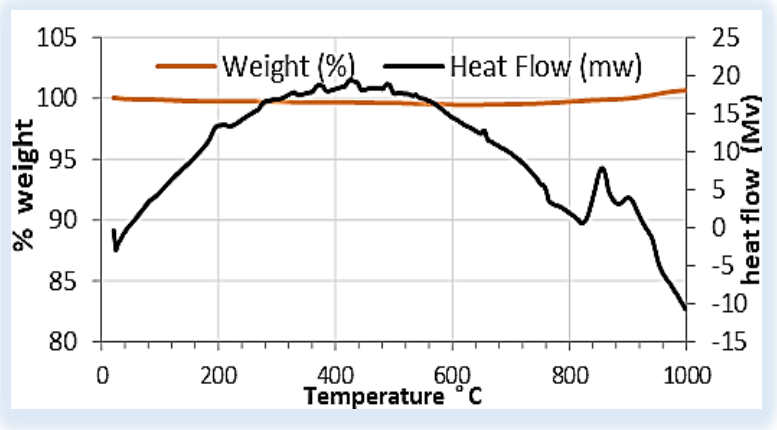

Figure 5. TGA and DSC analysis of the GGBS.

3.2. Setting times of the AA, GGBS mortars

All the activators produced similar setting times except for the NaOH activated slag which requires a significantly longer time to finally set (Table 6). The results agree with others in the literature (Table 6). Previous authors reported that, when the slag's SSA is under 450 m^2/kg, the binders set in 1-3 minutes and hence the material is impossible to pour (Talling and Brandstetr in [4]). However, despite the slag being ultrafine, the setting times are over one hour for all of the activators. According to Anderson and Gram [29], the fineness of the slag does not affect the setting time significantly between values ranging from 350-530 m^2/kg, but over these values the setting times are much shorter. Setting also depends on the basicity of the slag ($CaO+ MgO / SiO_2$): a higher basicity will likely result in shorter setting times regardless of the activator [30].

Table 6. Setting time for alkali activated slags.* Fernández-Jiménez and Puertas [31,32]; **Andersson & Gram [29]; +Zhang et al [7].

Activators	Initial time: t_i	Final time: t_f	$\blacktriangle t = t_i - t_f$	Slag properties	
				Fineness (m^2/kg)	Basicity
Na_2SiO_3	1h 11 min	1h 31 min	20 min		
Na_2SiO_3/NaOH	1h 8 min	1h 26 min	18 min	1950	1.56
NaOH	1h 15 min	2h 8 min	53 min		
*Na_2SiO_3	1h 16 min	1h 46 min	20 min		
*80%Na_2SiO_3/20%NaOH	1h 15 min	1h 55 min	25 min		
*NaOH	2h 45 min	3h 50 min	30 min	460	1.51
*80%NaOH/20%Na_2SiO_3	1h 10 min	1h 40 min	20 min		
**Na_2SiO_3	2h 20min	4h 45min	2h 25min		
**NaOH	3h 40min	4h 40 min	1h	550	1.40
+Na_2SiO_3	1 h 30 min	4h 20 min		701	1.48

3.3. Mechanical strength of the AA, GGBS mortars

Influence of activator. In general, the Na_2SiO_3 + NaOH activated slags tend to achieve the greatest compressive and flexural strengths (Table 7, Figure 6) agreeing with Fernández–Jiménez et al [6]. However, when cured at ambient temperature, the early strenghts (3 days) are superior for the NaOH activated slags. This has been previously reported and attributted to the slags reacting faster with the NaOH than the silica, hence

reaching greater early strengths [6]. The early strengths of the Na_2SiO_3 + NaOH materials are lower than some in the literature, probably due to the slag's ultrafine nature and high SSA: an increment in the SSA of the slag has a negative effect on strength with Na_2SiO_3 + NaOH activators [32].

The Na_2SiO_3 activated slags result in poor strengths disagreeing with previous studies [8, 12, 31-35]. The reason for the low strength is an excessive %Na_2O by mass of slag (the high reactivity of the slag would require a lower %Na_2O), as the optimum quantity lies between 3-6% by mass of slag, and the materials are over this threshold [5]. The strength of the NaOH activated slags is lower than Talling and Krivenko [36] most likely due to an excessive alkalinity, produced by an undue high molarity of the NaOH solution (the alkalinity being excessive for the highly reactive nature of the slag). The sporadic efflorescence observed in some of the materials conforms with the alkalinity being excessive, as efflorescence has been associated with high concentrations of hydroxide activator in slag materials [3-4]. The appearance of occasional microcracks also agrees with the high alkalinity.

In most instances, the strength tends to increase over time, raising significantly at late ages, between 28 and 270 days. The strength increase at late ages agrees with some authors such as Rodriguez et al. [37] who found strength increase up to 120 days, but does not conform with Collins and Sanjayan [38] who found that the strength of alkali activated slag concrete tends to reduce at late ages (360 days), and attributed the reduction to the occurrence of a network of interconnected microcracks with increasing age.

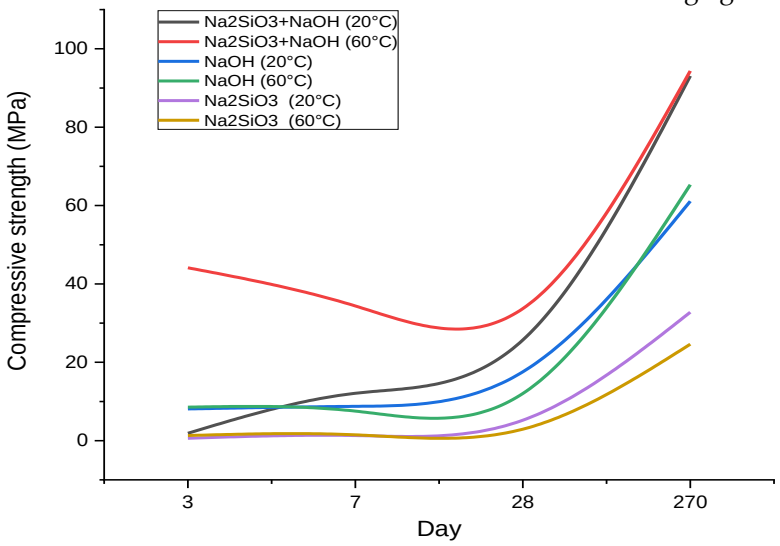

Figure 6. Effect of activator on compressive strength development.

Influence of curing temperature. A higher temperature is expected to increase the amount and rate of slag dissolution so that reactivity, and hence strength gain are favoured. The effect of increasing temperature for each of the activators is shown in figures 7-9. Increasing temperature, enhances strength when Na_2SiO_3+NaOH is the activator (mainly at early ages, up to 28 days, agreeing with former authors [6, 8, 31-34]) but can lower the ultimate strength when the NaOH and Na_2SiO_3 activators are used separately.

The general tendency is that raising the curing temperature enhances the strengths at early ages (3, 7 days) - except for the flexural strength of the NaOH activated slag which lowers-. However, at late ages (28, 270 days) the strength increase with rising temperature is less significant, and sometimes the ultimate strength lowers (e.g. the compressive strength of Na_2SiO_3 activated slag at 270 days lowers considerably when cured at 60°C). Yet, the tendency is that, the ultimate strength increase when rising the curing temperature is not significant, agreeing with former literature [6, 23]. Similarly, Bakharev et al. [39] report that heat initially accelerates the strength development of AA slag concrete, but at later ages, the compressive strength is reduced when compared with room

temperature curing. They observed that curing at 70°C accelerates early strength but, after 28 days, the strength was reduced by 35 to 45%.

Most of the strength variation triggered by the higher curing temperature is within the values reported by San Nicolas et al [40], who studied the performance of AA slag materials up to the age of 540 days and report total strength variations of around 5 MPa, and no significant ultimate strength variation with increasing curing temperature from 20 to 60°C.

The NaOH activator tends to perform best at room temperature agreeing with Fernández–Jiménez et al. [6] who note that an increase of temperature lowers the strength of NaOH-activated slags at all ages and with Altan and Erdoğan [12]. The 0.77 MPa result of the NaOH-activated slag is unreliable, and likely due to a defective specimen with microcracks).

Table 7. Compressive and flexural strengths of AA, GGBS materials: effect of the type of activator, curing temperature and age. 3:1 (sand:GGBS); Na_2SiO_3/NaOH=1.5; 8M NaOH.

	Flexural strength						**Compressive strength**					
Activator	**Na_2SiO_3+NaOH**		**NaOH**		**Na_2SiO_3**		**Na_2SiO_3+NaOH**		**NaOH**		**Na_2SiO_3**	
COVs	**0.05-0.13**		**0.00-0.20**		**0.01-0.41**		**0.10-0.48**		**0.00-0.23**		**0.05-0.29**	
Curing T	**20°C**	**60°C**	**20°C**	**60°C**	**20°C**	**60°C**	**20°C**	**60°C**	**20°C**	**60°C**	**20°C**	**60°C**
3 day	0.66	7.31	3.33	1.75	0.28	1.30	1.88	44.11	8.09	8.56	0.60	1.30
7 day	3.51	7.10	3.07	1.15	0.70	1.50	12.08	34.38	8.77	7.53	1.31	1.50
28 day	6.12	7.09	0.77	1.65	1.89	3.25	25.70	33.69	17.56	12.03	5.21	2.92
270 day	7.01	7.26	5.62	8.26	5.70	3.05	93.06	94.36	61.11	65.31	32.79	24.63
% change 28-270 d	+12	+2	+86	+80	+66	-6	+72	+64	+71	+81	+84	+88

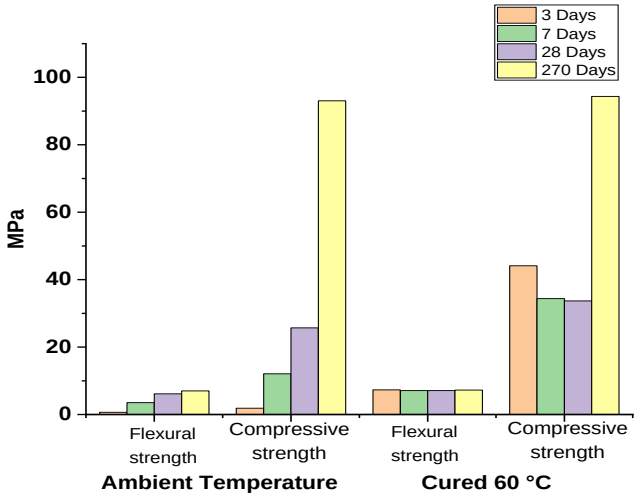

Figure 7. Strength development of the Na_2SiO_3+NaOH-activated, GGBS mortars.

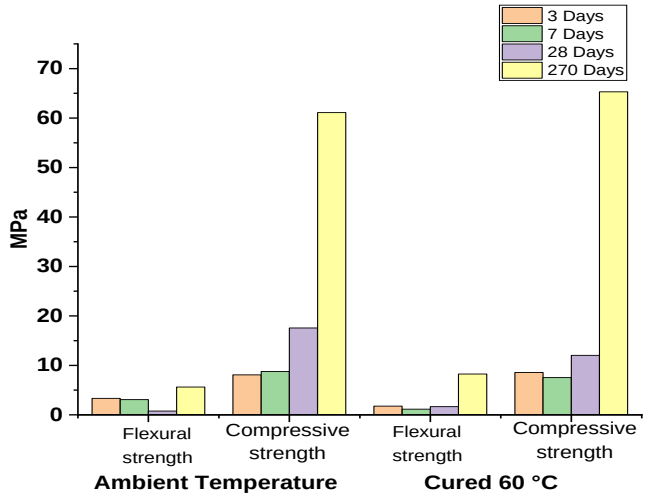

Figure 8. Strength development of the NaOH-activated, GGBS mortars.

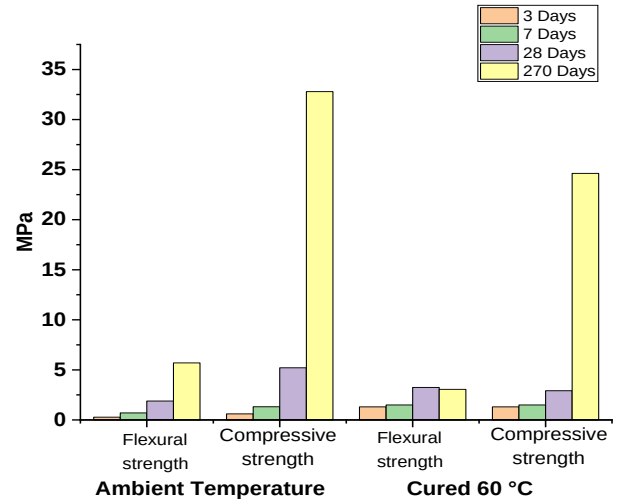

Figure 9. Strength development of the **Na_2SiO_3**-activated, GGBS mortars.

3.4 Microstructure of the Na_2SiO_3+NaOH activated, GGBS materials by petrographic and SEM analyses

The Na_2SiO_3+NaOH activated GGBS showed the best mechanical strength. Therefore, its microstructure was further investigated. In the alkali activation process, the activator dissolves the slag, sending Si^{4+}, Al^{3+} and Ca^{2+} into the interstitial solution, hence becoming available to form cements. As seen in the slag characterisation, the GGBS is mostly amorphous, consequently, nearly all the SiO_2, CaO and Al_2O_3 present in the original slag is reactive, and should participate in cement formation. As aforementioned, there is consensus on that the main reaction product of AA slags is an aluminium-substituted C-A-S-H type gel with a disordered, tobermorite-like, C-S-H (I) structure, with AFm phases as secondary reaction products (mainly identified in NaOH-activated binders), and the Si-containing, AFm-phase strätlingite in silicate-activated binders [7 and 15 - based on research by Wang, Zhou and others). Other phases reaction phases include hydrotalcite (in slags with sufficient MgO) and zeolites -gismondine and garronite-, in slags with high Al_2O_3 and low (<5%) Mg. Siliceous hydrogarnets such as katoite were also found in silicate-activated slags [19].

The resolution of the petrographic microscope is not enough to resolve microcristaline and amorphous gels such as C-A-S-H and C-S-H. However, it can determine secondary mineral reactions, new-formed mineral phases and cracking, as well

as other textural and compositional features. At 28 days, the petrographic analyses show a dense microstructure with few pores (figure 10). In the ambient-cured materials (figure 10a), there are abundant unreacted GGBS grains in an opaque groundmass with occasional patches of cement. However, in the oven-cured materials (figure 10b), the binder structure is more homogeneous and crystalline due to a more extensive reaction, the fine GGBS particles have completely hydrated and others show hydration rims. No alkali-aggregate reactions (AAR) or alkali-silica reactions (ASR) were evident at 28 days, not even microsilica (chert) sand has reacted with the alkaline binder. However, 28 days is likely too early for any AAR or ASR.

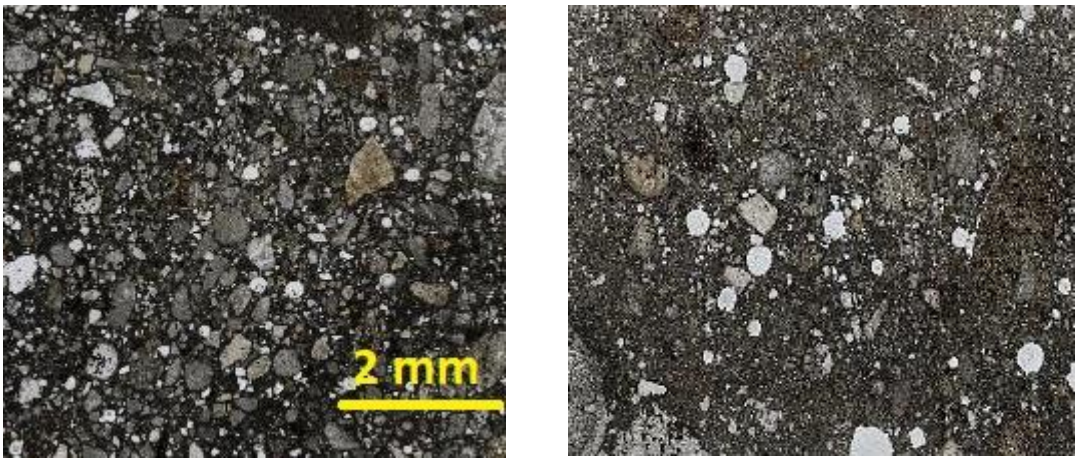

(**a**) (**b**)

Figure 10. General structure of the AA GGBS mortars at (28 days): (**a**) the ambient-temperature cured include abundant unreacted GGBS grains in an opaque binder groundmass; (**b**) the mortars cured at 60º C show considerably more reaction as the binder is slightly more crystalline, the finest GGBS particles have completely hydrated and others show hydration rims.

Ambient-cured, Na_2SiO_3+NaOH activated GGBS. The Backscattered-Electron (BSE) images (up to 28 days) showed unhydrated slag particles, hydration rims around slags, occasional hydrotalcite - $Mg_6Al_2(CO_3)(OH)_{16} \times 4H_2O$ -, and ghosts of fine, totally-hydrated GGBS particles (figures 11-12). The BSE images show elemental variations providing a clearer view of the mineral phases. Larger atoms scatter more electrons than light atoms, creating a superior signal and appearing brighter in the image. The hydration development follows features reported by Ben Haha et al [41], who activated ($NaOH/Na_2SiO_3$) slags of similar Al content (7-17wt.%) as those in the present study (12%wt): initially, the microstructure consists of bright unreacted slag grains in a homogeneous matrix, with no phase separation observable and some microcracking, presumably resulting from drying shrinkage (figure 11). As hydration progresses, the finest slags react, and a hollow-shell microstructure comparable to that formed on PC hydration is apparent sporadically, with outer hydration rims of C-S-H gels, inner products replacing slags, and relicts of unhydrous slags (figure 12). In the early stages, the SEM showed microcracks (figure 12) that were invisible with the naked eye and with the resolution of the petrographic microscope. However at later ages, the matrix becames more crystalline as it fills with hydrates, no coarse pores exist and the drying shrinkage cracking is reduced (figure 15). Cracking due to drying shrinkage is one of the challenges of alkali-activated slag materials, and it has been reported as the reason for the strength drop at late ages [12]. Cracking due to drying shrinkage is more prominent in systems with low lime content [2]. Hence, the high Ca content of this slag has probably reduced drying-shrinkage cracking in the long term and contributed to the sound microstructure of the materials [42].

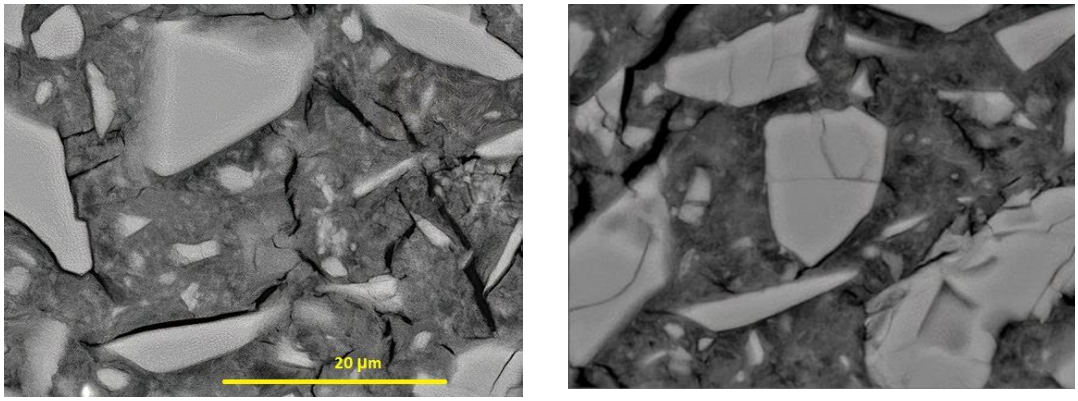

(**a**) (**b**)

Figure 11. BSE images of the early structure (2 weeks): (**a**) Unreacted slag and microcracks in the early structure; (**b**) Hydrate rims around fine slag grains and coarser unreacted slag.

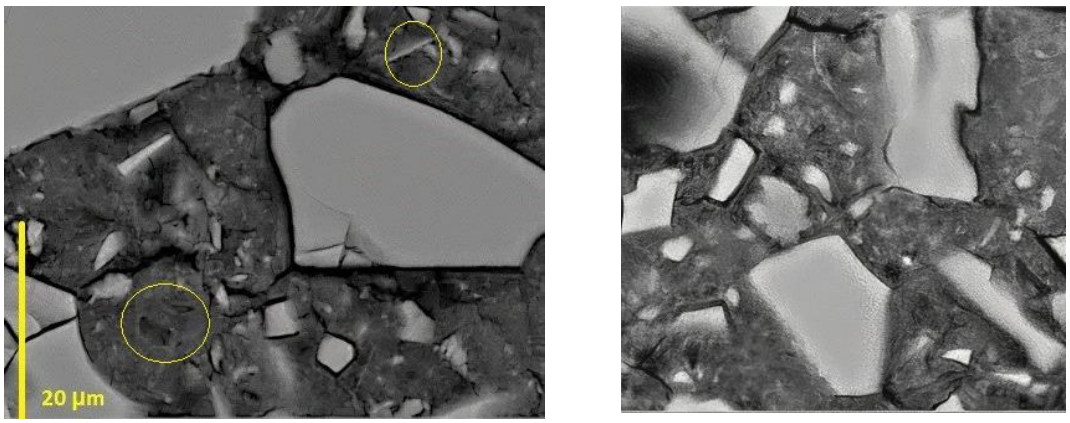

(**a**) (**b**)

Figure 12. BSE images of the structure at 28 days: (**a**) Ghost of fully-hydrated, fine slags and occasional hydrotalcite platelets; (**b**) Hydrated fine slags and hydrate rims around coarser slags.

The binder composition at 28 days, in the areas of figures 11-12, is displayed in table 8. The results are consistent with the high level of Al sustitution previously reported in the C-S-H cements of the AA slags. The Mg content agrees with the occasional hydrotalcite. There is some variation, as indicated by the standard deviation, and the low totals are due to the water content. The Na content is provided by the activator and picked up by the scattered EDX beam.

Table 8. Composition of the cements of the ambient-cured GGBS materials as %wt oxide.

	1	**2**	**3**	**4**	**5**	**6**	**St Dev**
SiO_2	32.0	30.4	33.5	30.3	24.4	29.2	2.69
Al_2O_3	8.93	7.95	7.78	8.12	7.61	7.61	0.50
CaO	21.8	20.8	21.7	22.1	19.4	19.6	1.46
NaO	1.79	1.62	1.55	2.05	2.03	1.49	0.47
MgO	4.63	3.48	3.53	3.84	3.30	4.25	0.62
K_2O	0.54	0.47	0.34	0.26	0.28	0.36	0.10
TiO_2	0.48	0.35	0.34	0.35	0.43	0.33	0.06
FeO	0.75	0.24	0.32	0.27	0.23	0.45	0.17
Total	71.0	65.3	69.2	67.3	57.7	63.3	3.96

Na_2SiO_3+NaOH-activated, GGBS materials cured at 60°C. The petrographic microscope shows a dense microstructure with no pores and abundant newformed cements (figure 13). However, their low crystallinity and lack of specific optical features makes identification difficult. Featureless C-S-Hs are very common (figure 13b-14). They are sometimes mixed with high relief and birrefringence phases that can be epidotes (figure 14). As aforementioned, Zhang et al. [7], found epidotes (zoisite and clinozoisite) and zeolites resulting from hydration of similar AA GGBS materials. Very small platy crystals of low birrefringence are possibly stratlingite and zeolites (figure 13). These phases have been identified by former authors in alkali-activated slag cements and lime-alumina-silica-hydrate systems [7, 19, 27, 43]. Zeolites of the gismondine family are often reported in AA cement systems, they are stable in the lime-alumina-silica-hydrate systems, compatible with C-S-H, strätlingite, katoite, silica, and aluminosilicate phases [43].

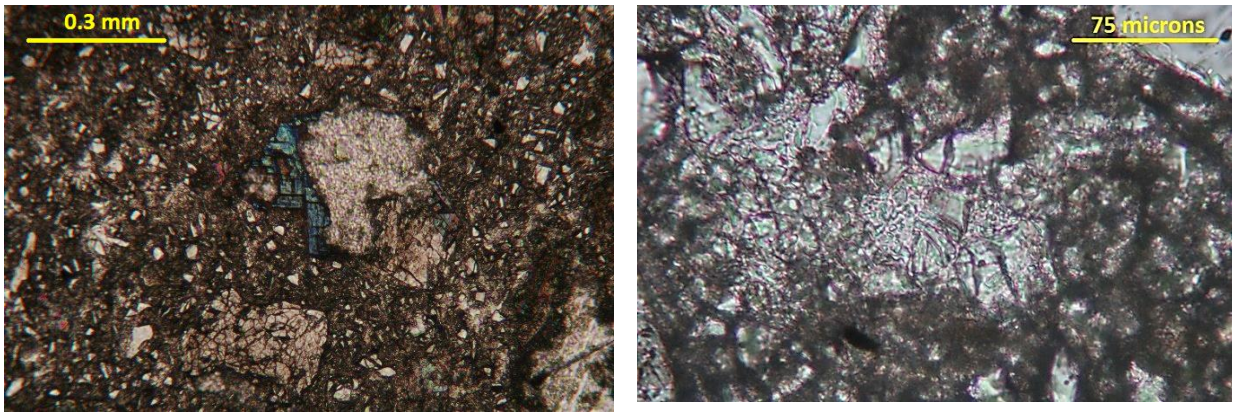

(**a**) (**b**)

Figure 13. Na_2SiO_3+NaOH-activated, GGBS materials cured at 60°C: (**a**) Dense mortar structure with no pores showing products of alkali reaction (centre). Polarised light 10X; (**b**) Detail of featureless C-S-H cements, remnants of un-hydrated slag and possible zeolite. Natural light 40X.

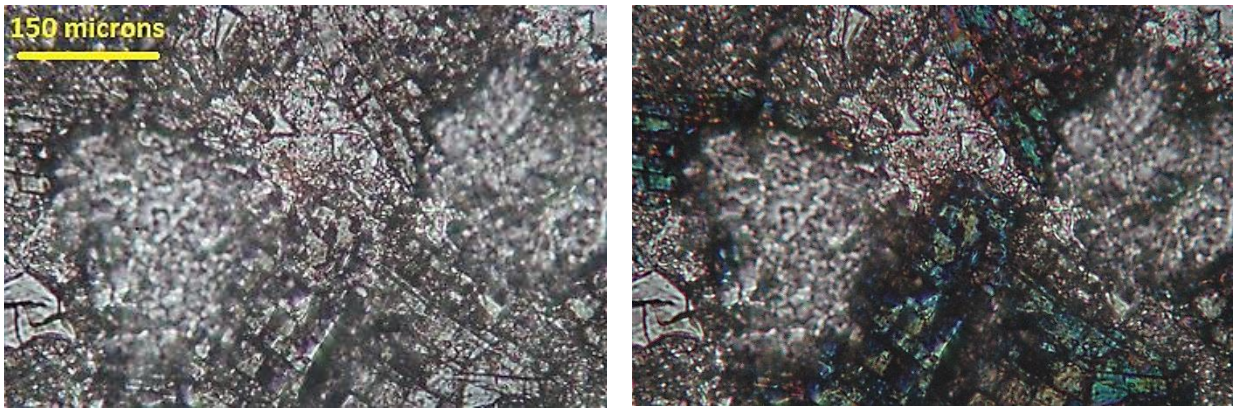

(**a**) (**b**)

Figure 14. Na_2SiO_3+NaOH-activated, GGBS materials cured at 60°C: (**a**) Detail of cements with C-S-H and epidote (high relief and cleavage), and scattered relics of un-hydrated slag. Natural light 20X; (**b**) Same image with polarised light showing the epidote's interference colour. Polarised light 20X.

The SEM showed abundant silicates with isometric and tabular habits, unreacted GGBS particles and randomly scattered C-S-H cements (figure 15a). The isometric phases are either octahedral or cubic, with occasional rounded aggregates of cubic crystals (figure 15b). The octahedral and cubic crystals are likely the garnet katoite, a member of the

$Ca_3Al_2(SiO_4)_3$- $Ca_3Al_2(SiO_4)_3$ $(OH)_{12}$, calcium aluminum silicate hydrate series of the hydrogrossular group (figure 15b, 16a). Katoite has been found in AA slag cements by former authors [15], and curing at 60°C has facilitated its appearance [44]. The presence of katoite agrees with Okoronkwo et al [43] who found that, in lime-alumina-silica-hydrate systems, at compositions of $CaO/Al_2O_3 + SiO_2 > 0.58$, katoite formation is favoured at 55 and 85°C instead of stratlingite or gismondine. The ratio of the GGBS in this study is $CaO/Al_2O_3 + SiO_2 = 0.95$.

The morphology and composition of the tabular blocky silicates suggest that they are gehlenite- Ca_2Al $[AlSiO_7]$ (figure 15a,16b). Gehlenite is the end polymorph of the GGBS, as shown in the devitrification experiment above, and it is in equilibrium with hydrogarnets. Hydrogarnet–gehlenite hydrate cements are reported by Liska et al. [45], on hydration of calcium aluminosilicate glasses containing 45%–55% CaO, 12%–26% SiO_2 and 22%–40% Al_2O_3. The presence of these phases is in agreement with the high Ca (42%), Al (12%) and Si (32%) content of this GGBS.

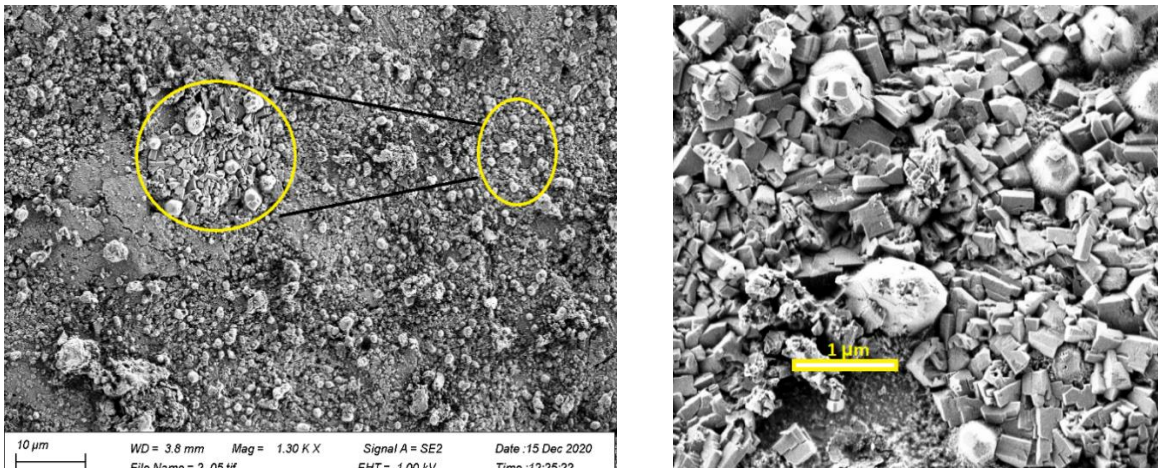

(**a**) (**b**)

Figure 15. Na_2SiO_3+NaOH-activated, GGBS materials cured at 60°C: (**a**) Microstructure with abundant hydrogarnet–gehlenite hydrate cements and occasional C-S-H cement.; (**b**) Detail of the hydrogarnet–gehlenite hydrate cements.

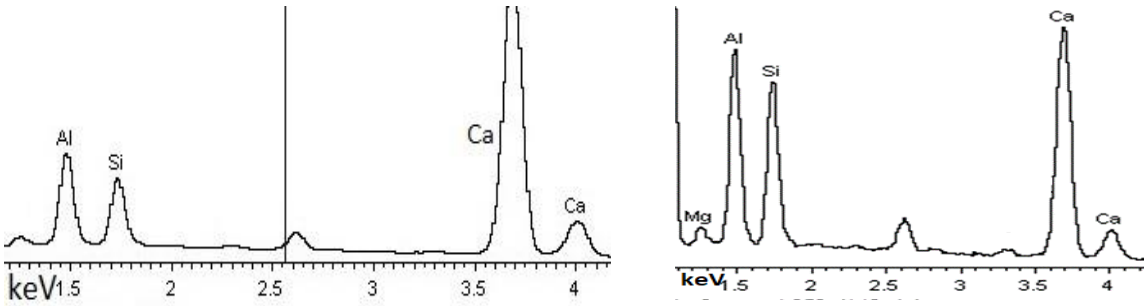

(**a**) (**b**)

Figure 16. Elemental composition of some crystals in the hydrogarnet–gehlenite hydrate cements: (**a**) isometric crystals of hydrogarnet; (**b**) tabular, blocky crystals of gehlenite.

4. Conclusion

The results indicate that the Irish GGBS can successfully produce AA materials. The GGBS shows outstanding qualities to produce AA binders being highly reactive and basic ($CaO+ MgO/SiO_2$ =1.56). Furthermore, it is highly amorphous, and has a CaO/SiO_2 ratio of

1.41 and a Al_2O_3/SiO_2 ratio of 0.34 which are considered suitable for alkali-activation. The devitrified mineral composition agrees with other active slags, comprising mainly melilite, in an isomorphous solid solution where the other end member is gehlenite. The GGBS complies with the standard requirements for use of slags in concretes, mortars and grouts. Despite being ultra-fine and highly reactive, the GGBS shows feasible setting times and minimal loss of workability. The rheology and setting times are within practical limits, comparable to values previously obtained in other AA slag-materials. Cracking due to drying shrinkage, one of the challenges of AA materials, is hindered thanks to the high calcium content of the slag.

The Na_2SiO_3+NaOH activated GGBS mortars showed the greatest mechanical properties and microstructure, when cured at 60°C, they develop hydrogarnet–gehlenite hydrate cements that may be responsible for their high strength at 270 days (94MPa).

Increasing the curing temperature to 60°C, enhances strength and microstructure when Na_2SiO_3+NaOH is the activator (mainly at early ages, up to 28 days) agreeing with former authors, but can lower ultimate strength when the NaOH and Na_2SiO_3 activators are used separately. The general tendency is that, the when rising the curing temperature to 60^0C, the early strengths (3, 7 days) are enhanced, but the ultimate strengths (28, 270 days) either slighly increase or reduce when compared with the ambient-cured materials, agreeing with former literature. The materials produced at ambient temperature are sound, and suitable for a wide range of applications.

Some of the strength values obtained when the NaOH and Na_2SiO_3 activators are used separately are lower than in the literature. The main reason for the strength loss when using the Na_2SiO_3 activator is an excessive $\%Na_2O$ by mass of slag, while for the NaOH activator is an excessive alkalinity of the solution (molarity is too high). The GGBS is too reactive (too fine and amorphous) for high alkali hydroxide concentrations. Therefore, the best activator is likely a combination of Na_2SiO_3 and a low molarity (<6M) alkali hydroxide.

Author Contributions: Omar Alelweet: laboratory testing and analysis, background research. Sara Pavia: research supervision, overall interpretation, writing.

Funding: We are tremendously grateful to the Government of Saudi Arabia and the SA Cultural Bureau for their support, and for financing the project.

Acknowledgments: We thank our subject librarian, D. MacNaughton, for his help with literary resources over the years. Also, J. Reddy of Ecocem, Dr. R. Goodhue and T. Dornan of TCD Geochemistry; Dr. A. Rafferty, Centre for Research on Adaptive Nanostructures and Nanodevices, TCD and Dr. J. Canavan, Geography Dept., TCD, for their assistance with the analyses. We thank our colleagues in the Civil Engineering laboratories M. O'Shea, M. Gilligan and P. Veale, in particular, M. Grimes and our Chief Technician D. McAuley and for their assistance with procuring materials and testing.

References

[1] Ouellet-Plamondon, C; Habert G. Life cycle assessment (LCA) of alkali-activated cements and concretes. In Book *Handbook of alkali-activated cements, mortars and concretes*, 1st ed; Woodhead Publishing, 2015, pp. 663–686.

[2] SHI, Caijun; ROY, Della; KRIVENKO, Pavel. Alkali-activated cements and concretes. CRC press, 2003.

[3] Pacheco-Torgal, F.; Labrincha, J., Leonelli, C.; Palomo, A.; Chindaprasit, P., *Handbook of alkali-activated cements, mortars and concretes*.1st ed; Publisher: Elsevier, Waltham, UK, 2014; PP. 111-419.

[4] Bernal, S. A.; Provis, J. L.; Fernández-Jiménez A.; Krivenko, P. V.; Kavalerova, E., Palacios, M..; Shi, C..Alkali activated materials, *Springer*, **2014**, 11-57.

[5] Hewlett P.; Liska M. *Lea's chemistry of cement and concrete*. 5th ed. ; Publisher: Hewlett, Butterworth-Heinemann-Elsevier, Oxford, UK, 1998; pp. 31-826.

[6] Fernández-Jiménez, A.; Palomo, J. G.; Puertas, F.. Alkali-activated slag mortars mechanical strength behavior. *Cement and Concrete Research* **1999**, Volume 29, 1313–1321.

[7] Zhang, Y. J.; Zhao, Y. L.; Li, H. H; Xu, D. L. Structure characterization of hydration products generated by alkaline activation of granulated blast furnace slag. *Journal of materials science* **2008**, Volume 43, no.22, 7141-7147.
[8] Bakharev, T.; Sanjayan, J. G.; Cheng, Y. B. Effect of admixtures on properties of alkali-activated slag concrete. *Cement and Concrete Research* **2000**, Volume 30, no. 9, 1367–1374.
[9] Liew, Y. M.; Heah, C. Y.; Mohd Mustafa, A. B.; Kamarudin, H. Structure and properties of clay-based geopolymer cements: A review. *Progress in Materials Science* **2016**, Volume 83, 595–629.
[10] Brough, A. R.; Atkinson, A. Sodium silicate-based, alkali-activated slag mortars: Part I. Strength, hydration and microstructure. *Cement and Concrete Research* **2002**, Volume 32, no. 6, 865–879.
[11] Bakharev T; Sanjayan, J. G.; Cheng, Y. B. Alkali activation of Australian slag cements. *Cement and Concrete Research* **1999**, Volume 29, no. 1, 113–120.
[12] Altan E.; Erdoğan S. T. Alkali activation of a slag at ambient and elevated temperatures. *Cement and Concrete Composites* **2012**, Volume 34, no. 2, 131–139.
[13] Fernández-Jiménez, A.; Puertas, F.; Sobrados, I.; Sanz, J. Structure of calcium silicate hydrates formed in alkaline-activated slag: influence of the type of alkaline activator. *Journal of the American Ceramic Society* **2003**, Volume 86, no. 8, 1389–1394.
[14] Puertas, F.; Palacios, M.; Manzano, H.; Dolado, J.S.; Rico, A., Rodríguez, J. A model for the CASH gel formed in alkali-activated slag cements. *Journal of the European Ceramic Society* **2011**, Volume 31, no. 12, 2043–2056.
[15] Provis, J. L.; Fernández-Jiménez, A., Kamseu, E.; Leonelli, C., ; Palomo, A. Binder chemistry–Low-calcium alkali-activated materials. *Alkali Activated Materials,* Springer **2014**, 93–123.
[16] Wang, S.D.; Scrivener, K.L.; Pratt, P.L. Factors affecting the strength of alkali-activated slag. *Cement and Concrete Composites* **1994**, Volume 24, no. 6, 1033–1043.
[17] Lothenbach, B.; Gruskovnjak, A. Hydration of alkali-activated slag: thermodynamic modelling. *Cement and Concrete Composites* **2007**, Volume 19, no. 2, 81–92.
[18] Chen, W.; Brouwers, H. The hydration of slag, part 1: reaction models for alkali-activated slag. *Journal of materials science* **2007**, Volume 42, no. 2, 428–443.
[19] Bernal, S.A.; Provis, J.L; Walkley, B.; San Nicolas, R.; Gehman, J.D.; Brice, D.G.; Kilcullen, A.; Duxson, P.; van Deventer, J.S.J. Gel nanostructure in alkali-activated binders based on slag and fly ash, and effects of accelerated carbonation. *Cement and Concrete Composites* **2013**. Volume 53, 127–144.
[20] Das, S. K.; Banerjee, S.; Jena, D. A review on geo-polymer concrete. *International Journal of Engineering Research & Technology* **2013**, Volume 2, no. 9, 2785–2788.
[21] EN 1015-3. Methods of Test for Mortar for Masonry. 1999.
[22] EN 196-3. Determination of Setting Times and Soundness. 2016.
[23] Wang, S. D.; Scrivener, K. L. Hydration Products of Alkali Activated Slag. 9th Int. Congr. *Cement and Concrete Research* **1995**, Volume 25, no. 3, 468–474.
[24] Puertas, F. Cementos de escorias activadas alcalinamente. Situación actual y perspectivas de future. *Materiales de Construcción,* **1995**, Volume 45,53-64.
[25] Moranville-Regourd M; Kamali-Bernard S. Cements made from blast furnace slag, *Lea's Chemistry of Cement and Concrete* **2019**, Volume 4, 469-507.
[26] Walker, R.; Pavía, S. Behaviour and Properties of Lime-Pozzolan Pastes. In *International Masonry Conference,* Dresden, July 2010.
[27] Bernal, S.A., Provis, J.L.; de Mejía Gutierrez, R.; Rose, V. Evolution of binder structure in sodium silicate-activated slag-metakaolin blends. *Cement and Concrete Research* **2011**, Volume. 33, no. 1, 46–54.
[28] Sha, W., Pereira, G. B. Differential scanning calorimetry study of ordinary Portland cement paste containing metakaolin and theoretical approach of metakaolin activity. *Cement and Concrete Composites* **2011**, Volume 23, no. 6, 455–461.
[29] Andersson, R.; Gram, H. E. Properties of alkali activated slag concrete. *Nordic concrete research* **1987**, Volume 6, 7–18.
[30] Krivenko, P. V. Influence of physico-chemical aspects of early history of a slag alkaline cement stone on stability of its properties. In *Proc. of 1st International Conference on Reinforced Concrete Materials,* Hot Climates, 1994.
[31] Fernández-Jiménez, A.; Puertas, F. Setting of alkali-activated slag cement. Influence of activator nature. *Advances in Cement Research* **2001**, Volume 13, no. 3, 115–121.
[32] Fernández-Jiménez, A.; Puertas, F. Effect of activator mix on the hydration and strength behaviour of alkali-activated slag cements. *Advances in cement research* **2003**, Volume 15, no. 3, 129–136.

[33] Atiş, C.D.; Bilim, C.; Çelik, Ö.; Karahan O. Influence of activator on the strength and drying shrinkage of alkali-activated slag mortar, *Construction and Building Materials* **2009**, Volume 23, no. 1, 548–555.
[34] Krizan, D. ; Zivanovic, B. Effects of dosage and modulus of water glass on early hydration of alkali–slag cements. *Cement Concrete Research* **2002**, Volume 32, no. 8, 1181–1188.
[35] Burciaga-Díaz, O.; Escalante-García, J. I. Structure, mechanisms of reaction, and strength of an alkali-activated blast-furnace slag. *Journal of the American Ceramic Society* **2013**, Volume 96, no. 12, 3939–3948.
[36] Talling, B.; Krivenko, P. Alkali activated slag cements from research to practice. *SCI meeting on AA slag cements* , London 17 June 1996.
[37] Rodríguez E., Bernal S.; Mejía de Gutiérrez R. y Puertas F. Alternative concrete based on alkali-activated slag. *Mater. Materiales de Construcción* **2008**, Volume 58, no. 291, 53–67.
[38] Collins, F. ; Sanjayan, J. G. Microcracking and strength development of alkali activated slag concrete. *Cement Concrete Research* **2001**, Volume 23, no. 4–5, 345–352.
[39] Bakharev T.; Sanjayan J. G. ; Cheng Y.-B. Effect of elevated temperature curing on properties of alkali-activated slag concrete. *Cement Concrete Research* **1990**, Volume 29, no. 10, 1619–1625.
[40] San Nicolas R., Bernal S. A.; Mejía de Gutiérrez R., van Deventer J. S.J.; Provis J. L. Distinctive microstructural features of aged sodium silicate-activated slag concretes. *Cement Concrete Research* 2014, Volume 65, 41–51.
[41] Kim, J. K.; Kim, J. S.; Ha, G. J.; Kim, Y. Y. Influence of slag chemistry on the hydration of alkali-activated blast-furnace slag—Part II: Effect of Al2O3. *Cement Concrete Research* **2012**, Volume 42, no. 1, 74–83.
[42] Alelweet O; Pavia S. Durability of Alkali-Activated Materials Made with a High-Calcium, Basic Slag. *Recent Progress in Materials* **2021**, Volume 3, no. 4.
[43] Okoronkwo MU; Mondal SK; Wang B, Ma H; Kumar A. Formation and stability of gismondine-type zeolite in cementitious systems. *Journal of the American Ceramic Society*, 2021, vol. 104, no. 3, pp. 1513–1525.
[44] Kyritsis K.; Meller N.; Hall, C. Chemistry and Morphology of Hydrogarnets Formed in Cement-Based CASH Hydro ceramics Cured at 200° to 350° C. *Journal of the American Ceramic Society* **2009**, Volume 92, no. 5, 1105–1111.
[45] LISKA, Martin; WILSON, Alexander; BENSTED, John. Special Cements. In *Lea's Chemistry of Cement and Concrete*, 5th ed.; Hewlett, PC, Liska, M., Eds, 2019, 618.
[46] Fernández-Jiménez, A.; Puertas, F. Effect of activator mix on the hydration and strength behaviour of alkali-activated slag cements. *Advances in cement research* **2003**, Volume 15, no. 3, 129–136.